Journal of Molecular Catalysis A: Chemical 344 (2011) 132–137

Contents lists available at ScienceDirect

Journal of Molecular Catalysis A: Chemical

journal homepage: www.elsevier.com/locate/molcata

Effect of synthesis method on the properties of ceria–zirconia modified alumina and the catalytic performance of its supported Pd-only three-way catalyst

Qiuyan Wang[a], Zhenguo Li[a,b], Bo Zhao[a], Guangfeng Li[a], Renxian Zhou[a,*]

[a] Institute of Catalysis, Zhejiang University, No. 148 Tianmushan Road, Hangzhou 310028, PR China
[b] China Automotive Technology & Research Center, No. 218 Chenglin Road, Tianjin 300162, PR China

ARTICLE INFO

Article history:
Received 24 March 2011
Received in revised form 14 May 2011
Accepted 14 May 2011
Available online 23 May 2011

Keywords:
Ceria–zirconia modified alumina
Different preparation methods
Textural/structural properties
Redox behavior
Pd-only three-way catalyst

ABSTRACT

In this paper, five types of ceria–zirconia modified alumina (CZA) were prepared by co-precipitation with supercritical drying (CPS), co-precipitation with common drying (CPC), sol–gel (SG), micro-emulsion (ME) and impregnation (IM) methods, respectively. The corresponding supported Pd-only three-way catalysts (TWC) were also prepared and evaluated in the simulative gasoline engine exhaust. The influence of different preparation methods on the physicochemical properties of CZA mixed oxide and its supported TWC was characterized by X-ray diffraction (XRD), N_2 adsorption/desorption and transmission electron microscopy (TEM) techniques. The redox behavior was investigated with H_2 temperature-programmed reduction (H_2-TPR) experiments. The results reveal that the CZA mixed oxides derived from CPS and ME methods exhibit the relatively higher textural and structural properties as well as better redox behavior, which lead to the better catalytic activity and wider air-to-fuel operation window of the corresponding Pd-only three-way catalysts.

1. Introduction

In the past decades, environmental protection has attracted an increasing world wide concern. It is well-known that gasoline engine exhaust is one of the main sources for air pollution [1–6]. Three-way catalytic converter represents a well established technology for the abatement of NO_x, CO and hydrocarbon (HC) emission from gasoline engine-powered vehicles. However, as a result of the tightened legislations relating to automobile exhaust, the production of novel three-way catalyst (TWC) is required, which is the core of the catalytic converter.

Classical components of TWC usually include Rh, Pt, and/or Pd as active metal, Ce–Zr mixed oxide as the promoter, and high-surface area alumina as the support [7–11]. Recently, the use of Pd as the only active metal in TWC has received considerable attention considering the economic factor (the high cost and scarcity of Rh) and the availability of clean fuel as well as its excellent capability for low-temperature oxidation of carbon monoxide and hydrocarbons [3,9,12]. In practice, alumina is usually used as support in order to maintain favorable dispersion of active metal [13,14]. However, alumina supported palladium catalysts are not stable under high temperature in the catalytic converter [15,16]. The deactivation of PdO/Al_2O_3 catalysts is reported to be mainly due to a decrease in the surface area of alumina and the transformation of PdO to Pd at extreme high temperature [17]. For these reasons, addition of a promoter in order to increase the thermal stability of the catalyst is considered as an attractive alternative to enhance the performance of TWC [18,19]. Among the numerous potential promoters, ceria–zirconia is the best known [20–25]. On the one hand, the addition of ceria–zirconia into alumina would lead to the increased thermal stability of the support and catalyst. On the other hand, ceria–zirconia exhibits fast oxygen mobility and high oxygen storage capacity, which play an important role in the purification of gasoline engine exhaust.

Up to now, a great deal of attention has been paid to investigate the physicochemical properties of ceria-zirconia modified alumina (CZA), and it was found that the preparation procedure strongly affects the characters of CZA and the catalytic performance of its supported TWC [26–30]. In this paper, five different methods were adopted to synthesize CZA and the supported Pd-only three-way catalysts were also prepared. The samples were characterized from a structural and textural point of view with techniques such as X-ray diffraction (XRD), N_2 adsorption/desorption and Transmission electron microscopy (TEM) examination. The redox properties of the samples were investigated by means of H_2 temperature-programmed reduction (H_2-TPR). The catalytic performances of the corresponding TWCs were also investigated under the simulated automobile exhaust. Purpose of this work is to elucidate the optimal synthesis method for the development of a thermal stable TWC.

* Corresponding author. Tel.: +86 571 88273290; fax: +86 571 88273283.
E-mail address: zhourenxian@zju.edu.cn (R. Zhou).

1381-1169/$ – see front matter.
doi:10.1016/j.molcata.2011.05.011

2. Experimental procedures

2.1. Sample preparation

The five types of ceria–zirconia modified alumina mixed oxides (CZA) were synthesized using co-precipitation with supercritical drying (CPS), co-precipitation with common drying (CPC), sol–gel (SG), micro-emulsion (ME) and impregnation (IM) methods, respectively. The content of ceria–zirconia oxide was 18 wt.% with Ce/Zr molar ratio of 3:1 in the sample.

In the co-precipitation with supercritical drying technique, the ammonia solution was slowly added to quantitatively mixed aqueous solution of $Ce(NO_3)_3$, $ZrO(NO_3)_2$ and $Al(NO_3)_3$ under continuous stirring until pH = 9.5. The resulting precipitate was filtered, extensively washed with distilled water, and then washed with ethanol furthermore to replace the water in the precipitate considering that it would be dried under supercritical condition in ethanol (250 °C, 7.5 MPa) subsequently.

The co-precipitation with common drying method was performed by an addition of aqueous ammonia into the mixture of corresponding nitrates drop by drop under continuous stirring until pH value achieved 9.5. The obtained deposition was filtered and washed with distilled water followed by drying at 110 °C for 12 h.

In the sol–gel preparation procedure, the citric acid solution was slowly added to quantitatively mixed aqueous solution of $Ce(NO_3)_3$, $ZrO(NO_3)_2$ and $Al(NO_3)_3$ followed by evaporating at 80 °C until a spongy and transparent yellow gel was gained. Then the gel was dried at 110 °C for 12 h.

For micro-emulsion preparation method, cetyltrimethylammonium bromide (CTAB) was quantitatively mixed with butanol and cyclohexane with stirring until the mixture became transparent. The acquired microemulsion was divided into two parts. One was mixed with the corresponding nitrates, and the other one was mixed with solution of aqueous ammonia. Then, the microremulsion containing aqueous ammonia was added to the other mixture under vigorous agitation until the solution was suspended with formed colloidal particles. After aging at room temperature (20 °C) overnight, the precipitate was filtered, washed with deionized water and dried at 110 °C for 12 h.

With regard to the impregnation method, ceria and zirconia were deposited by impregnation of the γ-Al_2O_3 with an aqueous solution of $Ce(NO_3)_3$ and $ZrO(NO_3)_2$. Then the slurry was vaporized with water bath method at 100 °C followed by drying at 110 °C for 12 h.

All the dried samples mentioned above were calcined at 500 °C for 4 h to gain the so-called fresh supports. In briefly, they are marked as CZA-CPS, CZA-CPC, CZA-SG, CZA-ME and CZA-IM, respectively. The samples were also calcined at 1100 °C for 4 h to investigate the thermal stability, and the aged samples were labeled as CZA-CPSa, CZA-CPCa, CZA-SGa, CZA-MEa and CZA-IMa, correspondingly.

The supported Pd-only three-way catalysts were prepared by conventional wet impregnation method with an aqueous of H_2PdCl_4 as metal precursor. The impregnated samples were reduced with hydrazine hydrate to de-associate Pd^{2+} and Cl^- via the transformation of Pd^{2+} to Pd. Then the reduced sample was filtered and washed with a large amount of deionized water until no Cl^- ion was detected in the filtered solution (by $AgNO_3$ aqueous) considering that the appearance of Cl is harmful to the catalytic activity. The washed samples were dried at 100 °C for 12 h and then calcined at 500 °C for 2 h due to the active phase in TWC was metal oxide. In order to investigate their thermal stability, the catalysts were also calcined at 1100 °C for 4 h. The theoretical loading content of Pd for the catalyst was 0.5 wt.%. The catalysts obtained at 500 °C were denoted as Pd/CZA-CPS, Pd/CZA-CPC, Pd/CZA-SG, Pd/CZA-ME and Pd/CZA-IM, respectively. The corresponding aged catalysts were labeled with an additional suffix "*a*" similarly.

2.2. Catalytic activity test

The evaluation of three-way catalytic activity was performed in a fixed-bed continuous flow quartz reactor. The catalyst (0.2 ml) was held in the quartz tube by packing quartz wool at both ends of the catalysts bed, and the back-mixing in reactor is minimized by decreasing the dead volume of the reactor. The feed stream was regulated using special mass flow controllers and contained NO (0.1%)–NO_2 (0.03%)–HC (0.033%)–CO (0.68%)–O_2 (1.745%) with balance Ar at a GHSV of 24,000 h^{-1} referred to the catalyst volume and to a gas flow rate at room temperature (25 °C). The contents of CO, NO, NO_2 and total HC (C_3H_6 and C_3H_8) were recorded by a Bruker EQ55 FTIR spectrometer coupled with a multiple reflection transmission cell (Infrared Analysis Inc.) before and after the simulated gas passed the reactor. The air/fuel ratio (λ) is defined as $\lambda = (2V_{O_2} + V_{NO} + 2V_{NO_2})/(V_{CO} + 9V_{C_3H_6} + 10V_{C_3H_8})$ (V means concentration in volume percent unit), $\lambda = 1$ was utilized in all the activity measurements and the air/fuel ratio experiment was carried out at 400 °C with adjusting the concentration of O_2.

2.3. Characterization techniques

Powder X-ray diffraction (XRD) patterns were recorded by a Rigaku D/Max-IIIB apparatus using Cu-Kα radiation operating at 45 kV and 40 mA with 0.02° step size scanning from 20° to 80° (2θ).

The Brunauer–Emmett–Teller (BET) specific surface areas of the samples were determined by nitrogen physisorption at 77 K using a Coulter OMNISORP-100 apparatus after degassing the samples in vacuum ($<10^{-5}$ Torr) at 200 °C for 2 h.

Transmission electron microscopy (TEM) examinations were operated on a JEOL JEM-2010 electron microscope operating at 200 kV. Portions of samples were crushed in an agate mortar and suspended in ethanol. After ultrasonic dispersion, a droplet was deposited on a copper grid supporting a perforated carbon film. Bright-field micrographs were recorded over selected areas.

H_2 temperature programmed reduction (H_2-TPR) measurements were carried out on a GC-1690 chromatography (KeXiao Chemical Instruments Co., Ltd., China) to observe the reducibility of the samples. Prior to H_2-TPR measurement, 50 mg catalyst was pretreated at 300 °C in air for 0.5 h. The reducing gas was a mixture of 5 vol.% H_2 in Ar (40 ml/min), which was purified using deoxidizer and silica gel. The experimental temperature was raised at a constant rate of 10 °C per minute. The consumption of hydrogen during the reduction reaction was measured by a thermal conductivity detector (TCD), and the water formed during H_2-TPR was absorbed with 5A molecular sieve.

3. Results and discussion

3.1. Textual and structural characterization

3.1.1. XRD

The XRD patterns of the fresh and aged samples are presented in Fig. 1, and the relevant lattice parameters are summarized in Table 1. What should be pointed out is that only lattice parameters and crystallite sizes of the main crystallite phase (ceria–zirconia solid solution) are shown in Table 1. From Fig. 1(a), it can be seen that the fresh samples consist of low intensity peaks from two phases: γ-Al_2O_3 and a major phase of cubic CeO_2 with the fluorite structure. In Fig. 1, no reflections ascribed to pure zirconia are observed. In addition, Table 1 shows that the lattice parameter of $Ce_xZr_{1-x}O_2$ is smaller than pure CeO_2 (a = 5.41 Å). This is due to the lattice shrinkage caused by the introduction of Zr^{4+} (0.84 Å), which

Table 1
Textural characteristic of the fresh and the aged samples prepared by different methods.

Samples	Fresh			Aged		
	S_{BET} (m^2/g)	Cell parameter (Å)	Crystalline size (nm)	S_{BET} (m^2/g)	Cell parameter (Å)	Crystalline size (nm)
CZA-CPS	358	5.3601	3.6	93	5.3644	16.1
CZA-CPC	252	5.3636	3.8	41	5.3655	18.5
CZA-SG	152	5.3702	3.2	22	5.3697	18.9
CZA-ME	257	5.3697	3.6	73	5.3652	16.3
CZA-IM	187	5.3806	5.8	27	5.3867	23.8

substitutes part of Ce^{4+} in the CeO_2 structure. Combined with the absence of clear zirconia peaks and the smaller lattice parameter, the formation of $Ce_xZr_{1-x}O_2$ solid solution could be indicated.

After calcination at 1100 °C for 4 h, the intensity of the XRD peaks for all the samples increases strongly, indicating the formation of larger crystallites caused by the extensive sintering. Although CZA-SG sample demonstrates a more nanostructure nature compared to the rest fresh samples, since its XRD pattern consists of lower intensity and more broadened peaks. However, the peak intensity and crystallite size of CZA-SG increase obviously after aging, indicating its poor thermal stability. For all the aged samples, no evidence for cubic CeO_2-rich and tetragonal ZrO_2-rich phase is found, which indicates that the phase separation of the ceria–zirconia solid solution does not take place. However, different transient alumina is observed for the aged samples. Fig. 1(b) shows that CZA-SGa and CZA-IMa comprise γ-Al_2O_3, δ-Al_2O_3 and α-Al_2O_3. With regard to CZA-CPSa, CZA-MEa and CZA-CPCa, no characteristic peaks of α-Al_2O_3 are observed. Based on the analysis presented above, we can conclude that CZA-CPS, CZA-ME and CZA-CPC show good thermal stability under high temperature. As displayed in Table 1, it is interesting that CZA-CPS and CZA-ME exhibit the relatively smaller grain size no matter before or after aging, indicating the better thermal stability of CZA prepared by co-precipitation with supercritical drying and micro-emulsion methods.

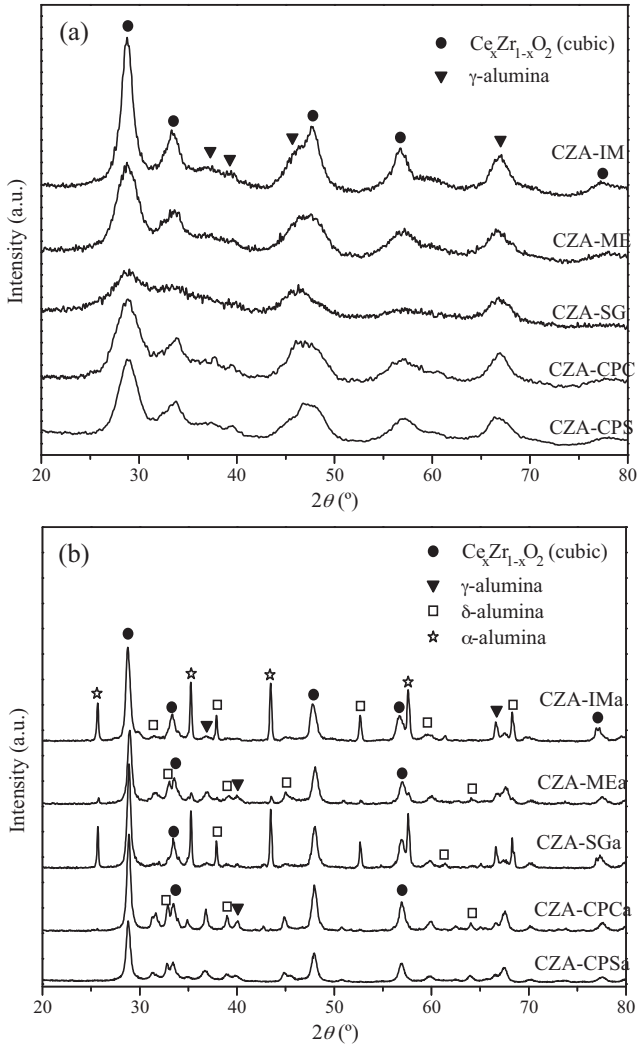

Fig. 1. XRD patterns for the fresh and aged CZA samples.

3.1.2. N_2 adsorption measurement

The values of the specific area calculated by BET method for all the samples are also shown in Table 1. For the fresh samples, CZA-CPS exhibits obviously larger specific surface area than others due to the adoption of supercritical drying technique, which can eliminate the vapor–liquid interface in the process of drying [31]. A clearly defined decrease in BET surface area is observed when comparing the aged samples with the fresh ones due to the sintering effects [32,33]. For the aged samples, the BET surface area of CZA-CPSa is 93 m^2/g, which is also the highest among all the aged samples. According to literature [25,34], the percentage loss of surface area from the fresh state to the aged one can be a measure of thermal stability. An examination of surface area data from Table 1 demonstrates that the surface area loss percentage ($\Delta S_{BET\%}$) is 74.02%, 83.73%, 85.53%, 71.60% and 85.56% for CZA-CPS, CZA-CPC, CZA-SG, CZA-ME and CZA-IM, respectively. This observation indicates that CZA-CPS and CZA-ME exhibit the relatively higher textural stability than the others.

3.1.3. TEM

To explore the structural evolution at atomic scale, studies by transmission electron microscope (TEM) are performed on all the fresh and aged Pd/CZA catalysts, and the obtained micrographs are given in Fig. 2. No explicit Pd can be visually identified on these TEM images due to the low metal loading (0.5 wt.%) and the high dispersion on the surface of support. It is only detected after a subsequent energy dispersive X-ray spectroscopy (EDS) analysis of a larger area. The images of fresh samples prepared by co-precipitation with supercritical drying, co-precipitation with common drying, and micro-emulsion methods show a homogenous material with sphere-like particles, and the sizes of these particles are almost the same as the crystallite sizes measured by XRD. For Pd/CZA-SG, the CZA particles are club-shaped, and the agglomeration is serious. With regard to Pd/CZA-IM, the particles are sheet-like with large size, indicating the deteriorated thermal stability. As shown by Fig. 2(b), (d), (f), (h) and (j), the sintering of samples occurs evidently after aging at 1100 °C, and the particle sizes of CZA become lager for the aged samples. However, the particle sizes of CZA-CPSa and CZA-MEa are relatively smaller than others, especially for CZA-CPSa, indicating the good anti-aging performance of CZA-CPSa and CZA-MEa.

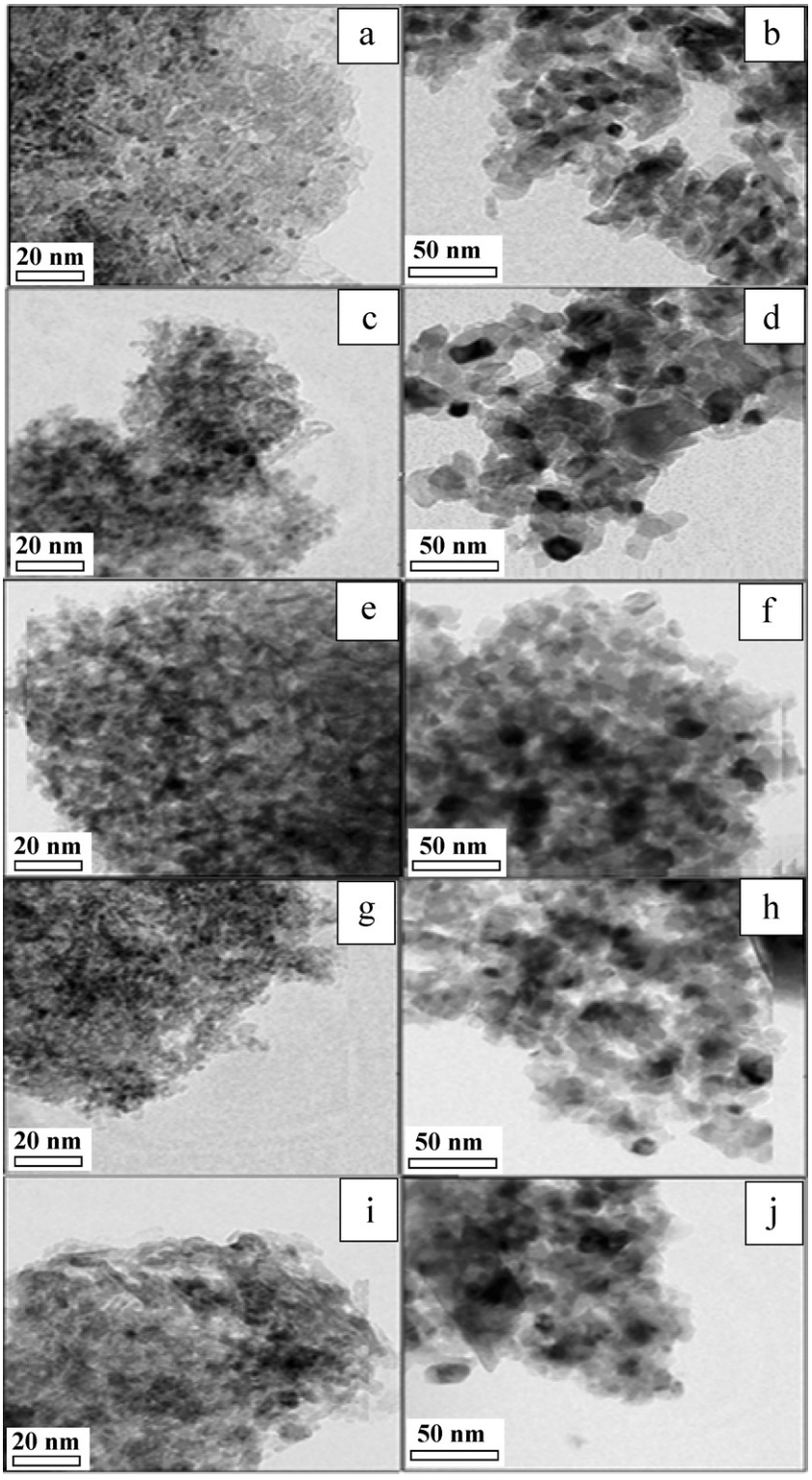

Fig. 2. The TEM photographs of Pd/CZA catalysts: (a) Pd/CZA-CPS; (b) Pd/CZA-CPSa; (c) Pd/CZA-CPC; (d) Pd/CZA-CPCa; (e) Pd/CZA-SG; (f) Pd/CZA-SGa; (g) Pd/CZA-ME; (h) Pd/CZA-MEa; (i) Pd/CZA-IM; and (j) Pd/CZA-IMa.

3.2. Temperature-programmed reduction

According to reports in the literature [35,36], the reducibility of supported palladium oxide is an important factor influencing its catalytic performance and temperature-programmed reduction technique is used as a common mode to study the reducibility of catalysts. The TPR profiles of the fresh and aged catalysts are shown in Fig. 3. From Fig. 3(a), it can be seen that all the fresh catalysts exhibit one or two reduction feature at lower temperature, which are designated as peak α and peak β. For Pd/CZA-CPS, only peak α is observed with maxima at 27 °C, which is suggested to the reduction of PdO species highly dispersed on the surface of the support [37]. For the others fresh catalysts, an additional peak β is detected, which is ascribed to the reduction of PdO species formed on the

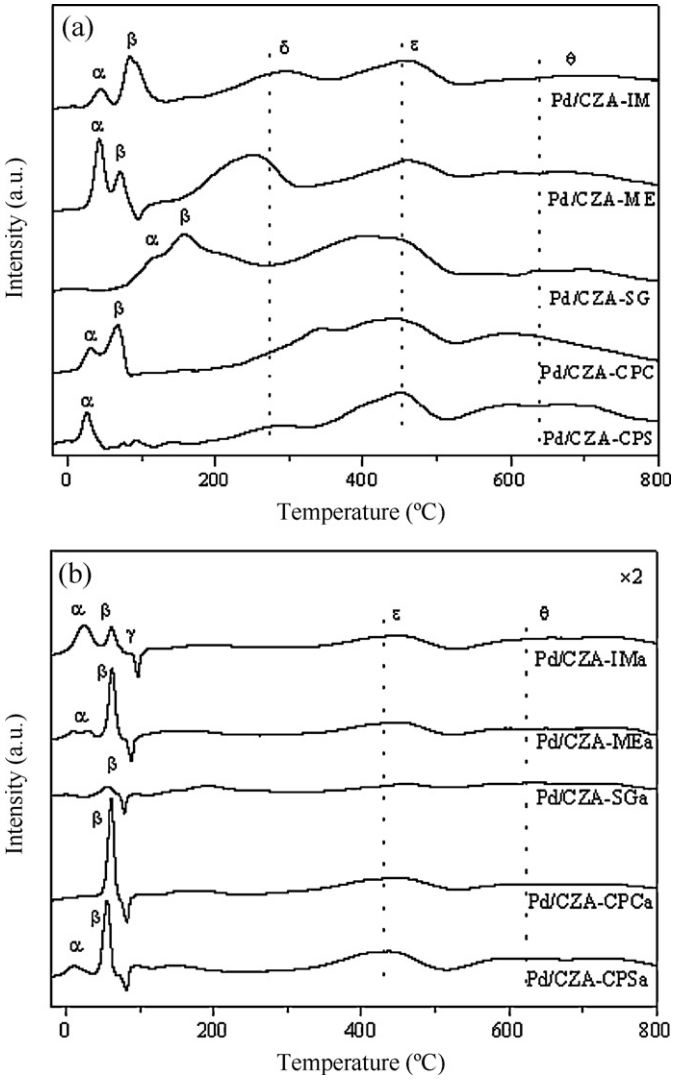

Fig. 3. The TPR response for the fresh (a) and aged (b) catalysts.

interface between PdO and the support [24,37]. These PdO species are in close contact with the support and have a strong interaction with it. Therefore, they are more stable than the highly dispersed PdO species. In addition, three broad peaks appear in the range of 200–800 °C are associated with the reduction of surface oxygen, sub-surface oxygen and bulk oxygen, respectively [38–40]. It is noticeable that the reduction temperature of peak α for Pd/CZA-CPS is the lowest among all the fresh catalysts, indicating that Pd/CZA-CPS shows the optimal reduction behavior. Similarly, from Fig. 3(a) we can conclude that Pd/CZA-SG exhibits the lowest reducibility.

After aging, the intensity of peak α decreases clearly due to the lower dispersion of active PdO species caused by the serious sintering during the aging process. With regard to Pd/CZA-CPCa and Pd/CZA-SGa, peak α is even absent, proving the distinct agglomeration of PdO species. Moreover, the intensity of peak β is very weak in the case of Pd/CZA-SGa. For Pd/CZA-CPCa, although the intensity of peak β is relatively stronger, the reduction temperature of peak β is higher than that of the other aged catalysts. It means that Pd/CZA-CPCa holds more stable PdO species. However, the reducibility of these PdO species is lower than that of the other catalysts. For Pd/CZA-IMa, the intensity of both peak α and peak β is weak, indicating the lower reducibility of Pd/CZA-IMa. On the contrary, the reduction temperature for PdO species (peak α and peak β) of Pd/CZA-CPSa and Pd/CZA-MEa is lower than the others and the intensity of peak β is relatively stronger. It indicates that more active PdO species are preserved on Pd/CZA-CPSa and Pd/CZA-MEa due to the good thermal stability. The negative peak at ca. 80 °C (peak γ) is generally attributed to the decomposition of palladium hydride formed following PdO reduction [41]. A careful comparison of fresh catalyst with the aged one shows that the surface oxygen in the range of 200–300 °C disappear after aging at 1100 °C for 4 h. The possible reason is the sintering of support in the process of high-temperature aging.

Table 2
Light-off temperature ($T_{50\%}$) and full-conversion temperature ($T_{90\%}$) of HC, CO, NO and NO_2 and the width of the operation window (W) over the fresh catalysts.

Sample	$T_{50\%}$ (°C)				$T_{90\%}$ (°C)				W
	HC	CO	NO	NO_2	HC	CO	NO	NO_2	
Pd/CZA-CPS	300	178	349	221	337	198	362	333	0.326
Pd/CZA-CPC	336	201	360	320	364	220	377	367	0.138
Pd/CZA-SG	315	195	357	272	348	208	371	359	0.233
Pd/CZA-ME	307	189	353	251	342	203	364	336	0.232
Pd/CZA-IM	322	219	357	264	351	228	372	349	0.139

3.3. Three-way catalytic activity performance

The catalytic activity performance of all the fresh and aged catalysts is performed in the simulated $CO + HC + NO + NO_2 + O_2$ mixture. The light-off temperature ($T_{50\%}$) and full-conversion temperature ($T_{90\%}$) of CO, HC, NO and NO_2 as well as the width of the air/fuel operation window (W) over all the fresh catalysts are summarized in Table 2. W (λ value width) acts as another scale to evaluate the property of catalyst when CO, HC and NO_x conversions all reach to 80% under rich and lean conditions. For example, the upper limit of stoichiometric windows is limited by NO_x conversion under rich condition; the lower limit is limited by CO conversion under lean condition for all samples. The upper limit subtracts the lower limit of λ is W value, and the bigger the W value is, the broader the three-way working window is.

From Table 2, it can be seen that all the catalysts are active in the conversion of simulated gasoline exhaust. The catalytic reaction started at ca. 300 °C and achieved completed conversion at 380 °C rapidly. What should be mentioned is that Pd/CZA-CPS shows the highest catalytic conversion for all the target pollutions, the $T_{50\%}$ and $T_{90\%}$ of which is the lowest among all the fresh catalysts. In addition, it also exhibits the widest air/fuel operation window. In general, the catalytic activity of all the fresh catalysts follows the sequence of Pd/CZA-CPS > Pd/CZA-ME > Pd/CZA-SG, Pd/CZA-IM > Pd/CZA-CPC. Moreover, the width of air/fuel operation window decreases as the sequence of Pd/CZA-CPS > Pd/CZA-ME, Pd/CZA-SG > Pd/CZA-IM, Pd/CZA-CPC. The main reason for the high three-way performance of Pd/CZA-CPS and Pd/CZA-ME can be the preferable homogenous structure and the higher redox behavior.

After aged at 1100 °C for 4 h, the lower of catalytic performance and the narrower of the air/fuel operation window are observed, and the related information are included in Table 3. Table 3 shows that only slight decrease of catalytic

Table 3
Light-off temperature ($T_{50\%}$) and full-conversion temperature ($T_{90\%}$) of HC, CO, NO and NO_2 and the width of the operation window (W) over the aged catalysts.

Sample	$T_{50\%}$ (°C)				$T_{90\%}$ (°C)				W
	HC	CO	NO	NO_2	HC	CO	NO	NO_2	
Pd/CZA-CPSa	318	205	341	284	353	226	356	349	0.283
Pd/CZA-CPCa	339	220	382	322	374	236	393	369	0.084
Pd/CZA-SGa	343	228	368	315	377	240	388	366	0.067
Pd/CZA-MEa	326	212	353	295	356	230	367	352	0.213
Pd/CZA-IMa	335	235	361	337	369	245	385	378	0.080

activity is detected for the aged catalysts when compared with the corresponding fresh one, indicating the excellent thermal stability of CZA system to PdO active species. Among all the aged catalysts, Pd/CZA-CPSa and Pd/CZA-ME also show higher catalytic activity to all the target pollutions and exhibit wider air to fuel operation window due to the good thermal stability of the support and the excellent redox behavior of the catalyst.

4. Conclusion

In this study, the effect of different preparation methods on the physicochemical properties of ceria–zirconia modified alumina and the three-way catalytic performance of its supported Pd-only catalyst have been investigated. The following conclusions can be put forward in view of the analysis mentioned above: (1) the ceria–zirconia modified alumina prepared by co-precipitation with supercritical drying method (CZA-CPS) and micro-emulsion method (CZA-ME) shows smaller crystallite size, bigger BET surface area and better thermal stability. (2) Pd/CZA-CPS and Pd/CZA-ME shows good redox behavior. (3) The preferable textural/structural properties of CZA-CPS and CZA-ME, and the higher redox behavior of Pd/CZA-CPS and Pd/CZA-ME lead to the relatively higher three-way catalytic performance and wider air/fuel operation window.

Acknowledgement

The authors acknowledge the Ministry of Science and Technology of China for the financial support of Project 2009AA064804. Moreover, they are also grateful to the Science and Technology Department of Zhejiang Province for the financial support of Project 2009R50020.

References

[1] L.N. Ikryannikova, A.A. Aksenov, G.L. Markaryan, G.P. Murav'eva, B.G. Kostyuk, A.N. Kharlanov, E.V. Lunina, Appl. Catal. A: Gen. 210 (2001) 225–235.
[2] H. He, H.X. Dai, L.H. Ng, K.W. Wong, C.T. Au, J. Catal. 206 (2002) 1–13.
[3] J. Kašpar, P. Fornasiero, N. Hickey, Catal. Today 77 (2003) 419–449.
[4] S.Y. Christou, A.M. Efstathiou, Top. Catal. 42–43 (2007) 415–419.
[5] I. Heo, J.W. Choung, P.S. Kim, I.S. Nam, Y.I. Song, C.B. In, G.K. Yeo, Appl. Catal. B: Environ. 92 (2009) 114–125.
[6] A. Papavasiliou, A. Tsetsekou, V. Matsouka, M. Konsolakis, I.V. Yentekakis, Appl. Catal. A: Gen. 382 (2010) 73–84.
[7] P. Fornasiero, R. Di Monte, G. Ranga Rao, J. Kašpar, S. Meriani, A. Trovarelli, M. Graziani, J. Catal. 151 (1995) 168–177.
[8] M. Ozawa, J. Alloys Compd. 275–277 (1998) 886–890.
[9] A. Martínez-Arías, M. Fernández-García, A.B. Hungría, A. Iglesias-Juez, K. Duncan, R. Smith, J.A. Anderson, J.C. Conesa, J. Soria, J. Catal. 204 (2001) 238–248.
[10] A.B. Hungría, N.D. Browning, R.P. Erni, M. Fernández-García, J.C. Conesa, J.A. Pérez-Omil, A. Martínez-Arías, J. Catal. 235 (2005) 251–261.
[11] A. Morikawa, T. Suzuki, T. Kanazawa, K. Kikuta, A. Suda, H. Shinjo, Appl. Catal. B: Environ. 78 (2008) 210–221.
[12] R.S. Monteiro, L.C. Dieguez, M. Schmal, Catal. Today 65 (2001) 77–89.
[13] P.O. Thevenin, E. Pocoroba, L.J. Pettersson, H. Karhu, I.J. Väyrynene, S.G. Järås, J. Catal. 207 (2002) 139–149.
[14] R. Spinicci, A. Tofanari, Appl. Catal. A: Gen. 227 (2002) 159–169.
[15] L. Matín, J.L. Arranz, O. Prieto, R. Trujillano, M.J. Holgado, M.A. Galán, V. Rives, Appl. Catal. B: Environ. 44 (2003) 41–52.
[16] M.V. Twigg, Appl. Catal. B: Environ. 70 (2007) 2–15.
[17] B. Yue, R. Zhou, Y. Wang, X. Zheng, Appl. Catal. A: Gen. 295 (2005) 31–39.
[18] L.F. Liotta, G. Deganello, D. Sannino, M.C. Gaudino, P. Ciambelli, S. Gialanella, Appl. Catal. A: Gen. 229 (2002) 217–227.
[19] M.A. Fraga, E. Soares de souza, F. Villain, L.G. Appel, Appl. Catal. A: Gen. 259 (2004) 57–63.
[20] M. Fernández-García, A. Martínez-Arias, A. Iglesias-Juez, A.B. Hungría, J.A. Anderson, J.C. Conesa, J. Soria, J. Catal. 214 (2003) 220–233.
[21] X. Wang, L. Xu, D. Weng, Appl. Surf. Sci. 221 (2004) 375–383.
[22] B. Yue, R. Zhou, Y. Wang, X. Zheng, J. Mol. Catal. A: Chem. 238 (2005) 241–249.
[23] T. Kuznetsova, V. Sadykov, L. Batuev, E. Moroz, E. Burgina, V. Rogov, V. Kriventsov, D. Kochubey, J. Nat. Gas. Chem. 15 (2006) 149–163.
[24] P.S. Lambrou, A.M. Efstathiou, J. Catal. 240 (2006) 182–193.
[25] A. Papavasiliou, A. Tsetsekou, V. Matsouka, M. Konsolakis, I.V. Yentekakis, N. Boukos, Appl. Catal. B: Environ. 90 (2009) 162–174.
[26] J. Noh, O.-B. Yang, D.H. Kim, S.I. Woo, Catal. Today 53 (1999) 575–582.
[27] M. Fernández-García, A. Martínez-Arias, A. Iglesias-Juez, A.B. Hungría, J.A. Anderson, J.C. Conesa, J. Soria, Appl. Catal. B: Environ. 31 (2001) 39–50.
[28] A.I. Kozlov, D.H. Kim, A. Yezerets, P. Andersen, H.H. Kung, M.C. Kung, J. Catal. 209 (2002) 417–426.
[29] X. Wu, B. Yang, D. Weng, J. Alloys Compd. 376 (2004) 241–245.
[30] C.C. Chuang, H.I. Hsiang, J.S. Hwang, T.S. Wang, J. Alloys Compd. 470 (2009) 387–392.
[31] Q. Wang, G. Li, B. Zhao, R. Zhou, Appl. Catal. B: Environ. 100 (2010) 516–528.
[32] J.R. Kim, W.J. Myeong, S.K. Ihm, Appl. Catal. B: Environ. 71 (2007) 57–63.
[33] H. Birgersson, L. Eriksson, M. Boutonnet, S.G. Järås, Appl. Catal. B: Environ. 54 (2004) 193–200.
[34] X. Wang, G. Lu, Y. Guo, L. Jiang, Y. Guo, C. Li, J. Mater. Sci. 44 (2009) 1294–1301.
[35] S.C. Su, J.N. Carstens, A.T. Bell, J. Catal. 176 (1998) 125–135.
[36] W. Lin, Y.X. Zhu, N.Z. Wu, Y.C. Xie, I. Murwani, E. Kemnitz, Appl. Catal. B: Environ. 50 (2004) 59–70.
[37] G.F. Li, B. Zhao, Q.Y. Wang, R.X. Zhou, Appl. Catal. B: Environ. 97 (2010) 41–48.
[38] I. Atribak, A. Bueno-López, A. García-García, J. Catal. 259 (2008) 123–132.
[39] J.Q. Wang, M.Q. Shen, Y. An, J. Wang, Catal. Commun. 10 (2008) 103–107.
[40] M.W. Zhao, M.Q. Shen, J. Wang, J. Catal. 248 (2007) 258–267.
[41] G. Chen, W.T. Chou, C.T. Yeh, Appl. Catal. 8 (1983) 389–397.